Change of the cerebrospinal fluid volume during brain activation investigated by $T_{1\rho}$-weighted fMRI

Tao Jin [a,*], Seong-Gi Kim [a,b]

[a] Department of Radiology, University of Pittsburgh, Pittsburgh, PA 15203, USA
[b] Department of Neurobiology, University of Pittsburgh, Pittsburgh, PA 15203, USA

ABSTRACT

A voxel in MRI often contains tissue as well as cerebrospinal fluid (CSF). During functional stimulation, volume fractions of these different water compartments may change. To directly image the CSF volume fraction and measure its functional change, we utilized a rotating-frame longitudinal relaxation time ($T_{1\rho}$)-weighted MRI technique. At 9.4 T with a spin-locking frequency of ~ 500 Hz, $T_{1\rho}$ of tissue water and CSF are about 48 and 450 ms, respectively. Therefore, the parenchyma signal becomes negligible when a long spin-locking time (e.g., 200 ms) is applied, leaving only the CSF signal. Baseline CSF volume fraction (V_{csf}) and its change induced by visual stimulation were mapped in isoflurane-anesthetized cats ($n = 6$). In both $T_{1\rho}$-weighted fMRI with spin locking times of 200 and 300 ms, negative changes with similar magnitudes were observed, indicating that a decrease in V_{csf} is a dominant contributor. In the region with voxels containing the visual cortex and CSF compartments, an average baseline V_{csf} was $24.6 \pm 2\%$, an average CSF volume fraction change ($\Delta V_{csf}/V_{csf}$) was $-2.45 \pm 0.6\%$, and an absolute change in CSF volume fraction (ΔV_{csf}) was $-0.6 \pm 0.15\%$. A negative correlation was observed between pixel-wise baseline V_{csf} and $\Delta V_{csf}/V_{csf}$, which can be explained by similar ΔV_{csf} among voxels. Our results suggest that the functional reduction of CSF volume fraction could contribute to fMRI signals, especially when the tissue signal is significantly reduced as compared to the CSF with certain experimental techniques or parameters.

Published by Elsevier Inc.

Introduction

The foundation of the current functional magnetic resonance imaging (fMRI) techniques lies in the change of hemodynamics, including an elevation in the cerebral blood flow (CBF) and volume (CBV) in response to neuronal activities. The functional increase in CBV would indicate a corresponding reduction of the volume of other brain compartments, such as tissue and cerebrospinal fluid (CSF), under the constraint of intracranial brain volume dictated by the Monro–Kelly doctrine. Since CSF acts as a buffer for the brain cortex and is more compliant compared to the tissue, it is plausible that the local CSF volume is adjusted to accommodate vascular dilation and/or tissue swelling. However, it remains unclear whether local CSF volume change is significant and whether it affects fMRI signals.

Recently, there have been a few studies examining changes in CSF volume fraction during stimulation (Donahue et al., 2006; Piechnik et al., 2009; Scouten and Constable, 2008). In a magnetic resonance spectroscopic study on human visual cortex at 3 T, a 5–6% and a 3% decrease of the CSF signal was observed under visual stimulation and CO_2 inhalation, respectively (Piechnik et al., 2009). Donahue et al. (2006) applied an MRI method with simultaneous nulling of blood and CSF signals and reported a functional decrease of CSF volume fraction from 10.7% to 10.1% during human visual stimulation, but the change was not statistically significant. With separated acquisitions of blood-nulled and CSF-nulled MRI, Scouten and Constable found that a majority of brain voxels underwent a 2–5% decrease of CSF volume fraction during breath-hold, while the change of CSF volume fraction was negligible or slightly positive near the visual cortex area (Scouten and Constable, 2008). In all aforementioned reports, the MR signal has contributions from more than one compartment; thus, determination of the CSF volume fraction relies on robust model-fitting procedures. The discrepancy of CSF volume fraction change at the visual cortex may be due to a limited signal-to-noise ratio (SNR) or data fitting errors. Therefore, it would be valuable to develop a method without data fitting for mapping functional changes of CSF volume fraction with high sensitivity.

Functional change of CSF volume fraction, if confirmed, would affect the interpretation of fMRI measurements, especially in the case where the parenchymal signal is significantly reduced relative to CSF. For example, in recent vascular space occupancy (VASO) or the gray matter-nulled inversion recovery fMRI techniques (Donahue et al., 2006; Lu et al., 2003; Shen et al., 2009), either the blood or the gray matter signal is nulled, whereas the CSF signal is still largely present. The quantification of relative CBV change could have an error as large as 15-fold if the change of CSF volume fraction is not taken into

* Corresponding author. Department of Radiology, University of Pittsburgh, 3025 E Carson Street, Pittsburgh, PA 15203, USA. Fax: +1 412 383 6799.
E-mail address: taj6@pitt.edu (T. Jin).

account (Scouten and Constable, 2008). Therefore, accurate measurement of functional CSF volume fraction changes is essential for the interpretation of fMRI signals.

In this work, we aimed (i) to develop a simple paradigm to image the CSF compartment directly and also (ii) to detect the functional change of CSF volume fraction. To suppress the parenchyma signal, a spin-locking (SL) MRI technique (see Fig. 1) was applied. During the SL period, MR signals decay by longitudinal relaxation time in the rotating frame ($T_{1\rho}$). Since the $T_{1\rho}$ of tissue water is much shorter than that of the CSF, the parenchyma signal becomes negligible when a long spin-locking time (TSL) is applied, leaving only the CSF signal. We measured functional changes in CSF volume fractions in isoflurane-anesthetized cats during visual stimulation and determined the relationship between CSF volume fraction at rest and its functional change.

Theoretical background

Determination of baseline CSF volume fraction

The pulse sequence for SL experiments is a double spin-echo EPI sequence with a non-selective SL preparation pulse (Grohn et al., 2005), where a 2-ms adiabatic half passage pulse is followed by a ramp of 0.5 ms (Fig. 1), during which the RF amplitude decreases to the desired SL field ($B_{1, SL}$), then by a constant spin-locking pulse with a duration of TSL. Following the SL preparation, transverse spins are refocused using two adiabatic full-passage RF pulses with slice-selection gradients. Surface coil setups have been used in many $T_{1\rho}$ studies (Borthakur et al., 2004; Grohn et al., 2005; Hakumaki et al., 2002; Koskinen et al., 2006; Makela et al., 2004; Xu et al., 2008), where the adiabatic SL pulse is essential to nutate all the spins within our area of interest to the transverse plane.

For an imaging voxel containing different water compartments, the MR signal acquired with the sequence in Fig. 1 can be written as

$$S = \sum_i V_i \cdot \rho_i \cdot M_0 \cdot (1 - e^{-TR/T_{1,i}}) \cdot e^{-TSL/T_{1\rho,i}} \cdot e^{-TE/T_{2,i}}, \quad (1)$$

where i represents the tissue, arterial blood, venous blood, and CSF compartments; V and ρ are the volume fraction and the proton density of each compartment, respectively; M_0 is the fully relaxed magnetization, which is considered to be 1.0; TR, TSL, and TE are the repetition, spin-locking, and echo times; and T_1, $T_{1\rho}$, and T_2 are the longitudinal, rotating-frame longitudinal, and transverse relaxation times, respectively. The $T_{1\rho}$ value of each water compartment is

dependent on the spin-locking frequency ($\nu_{1, SL} = \gamma B_{1, SL}$) and is approaching T_2 when the spin-locking frequency is low.

To measure the CSF volume fraction, an SL experiment can be performed with multiple TSL values. For simplicity, tissue and blood pools are considered as the "parenchyma" compartment, since arterial and venous blood volume fractions are small and their relaxation times are much closer to those of tissue compared to CSF. Thus, the MR signal is composed of the CSF and parenchymal compartments as:

$$S = V_{csf} \cdot S_{0, csf} \cdot \exp(-TSL/T_{1\rho, csf}) + (1 - V_{csf}) \cdot S_{0, par} \cdot \exp(-TSL/T_{1\rho, par}), \quad (2)$$

where $S_{0, i} = \rho_i \cdot (1 - \exp(-TR/T_{1, i})) \cdot \exp(-TE/T_{2, i})$ for the CSF (csf) and parenchyma (par). To estimate V_{csf} from multiple TSL MR data using the two-compartment model, the spin density, T_1, and T_2 of the CSF and parenchyma are obtained from the literature. In parenchymal voxels without CSF, $T_{1\rho, par}$ can be determined by fitting multiple TSL data with a single exponential function. Similarly, to calculate $T_{1\rho, csf}$, only data with long TSL should be used for single exponential fitting, assuming that non-CSF signals are suppressed at such long TSL values. In our studies, data with TSL ≥ 180 ms were used for measuring $T_{1\rho, csf}$, and the CSF-containing pixels were chosen using an intensity threshold (i.e., $S_{TSL=180\ ms} \geq 5\%$ of $S_{TSL=0\ ms}$).

Determination of functional change in CSF volume fraction

When a long TSL preparation pulse is applied, the parenchymal signal is suppressed, and the remaining signal can be described as

$$S \approx V_{csf} \cdot \rho_{csf} \cdot (1 - e^{-TR/T_{1,csf}}) \cdot e^{-TSL/T_{1\rho,csf}} \cdot e^{-TE/T_{2,csf}}. \quad (3)$$

Assuming no change in ρ_{csf} and $T_{1, csf}$, the fractional signal change during brain activation can be written approximately as

$$\Delta S/S \approx \frac{\Delta V_{csf}}{V_{csf}} - TSL \cdot \Delta R_{1\rho,csf} - TE \cdot \Delta R_{2,csf}$$
$$= \frac{\Delta V_{csf}}{V_{csf}} - f(TSL, TE) \quad (4)$$

Functional change of a heavily $T_{1\rho}$-weighted MR signal reflects (i) the modulation of the CSF volume fraction ($\Delta V_{csf}/V_{csf}$) as well as (ii) contributions of CSF $R_{1\rho}$ ($= 1/T_{1\rho}$) and R_2 ($= 1/T_2$) changes, if any. In our preliminary study (Jin et al., 2009), we have found that the $R_{1\rho}$ value obtained with a SL frequency of ~500 Hz is almost unaffected by variations in intravascular susceptibility effect. Since the functional signal induced by both relaxation terms (Eq. (4)) is linearly changed by proportionally modulating TSL and TE together, $\Delta V_{csf}/V_{csf}$ can be obtained from two fMRI data with different sets of TSL and TE values. For example, both TSL and TE values in the second fMRI run can be 50% or 100% higher than those of the first fMRI run. Then, $\Delta V_{csf}/V_{csf}$ can be separated from the $f(TSL,TE)$ term and can be converted into absolute ΔV_{csf} by multiplying baseline V_{csf}.

Materials and methods

Animal experiments

The animal protocol was approved by the Institutional Animal Care and Use Committee at the University of Pittsburgh. Six female adolescent cats, weighing from 1.28 to 2.0 kg, were used. Cats were initially treated with atropine sulfate (0.05 mg/kg, I.M.) and anesthetized with a cocktail of ketamine (10–25 mg/kg, I.M.) and xylazine (1–2 mg/kg, I.M.). The animals were then orally intubated and artificially ventilated. Gaseous anesthesia (2.0–2.2% isoflurane in a mixture of 70% medical air and 30% oxygen) was used during surgery. The femoral vein or cephalic vein was cannulated to deliver
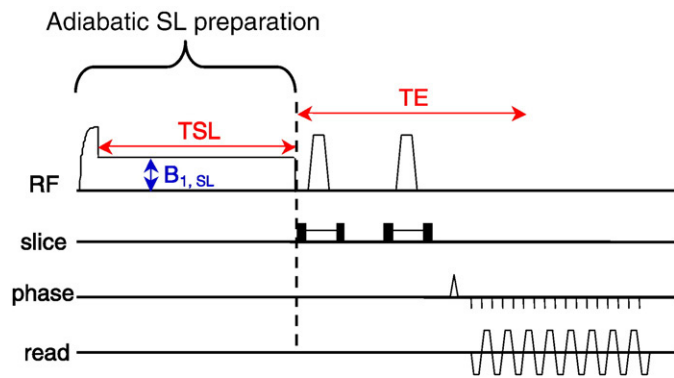

Fig. 1. Adiabatic version of spin-lock MRI pulse sequence. SL preparation for a surface coil is achieved by appending a continuous wave SL pulse ($\nu_{1, SL} = \gamma B_{1, SL}$) immediately after an adiabatic excitation pulse that initially rotates the magnetization to the transverse plane. After the adiabatic SL preparation, a double refocused spin-echo EPI image is acquired. Adiabatic full-passage pulses are applied with slice-selection gradients. Small crush gradients are used before and after 180° pulses. TSL: spin-locking time; $B_{1,SL}$: spin-locking B_1; TE: echo time.

pancuronium bromide (0.2 mg/kg per hour) and maintenance fluid. In terminal experiments, one femoral artery was catheterized to monitor the arterial blood pressure and to obtain blood samples for arterial blood gas measurements. During fMRI experiments, the isoflurane level was reduced to $1.0 \pm 0.2\%$. End-tidal CO_2 level was kept within $3.5 \pm 0.5\%$, and the rectal temperature was controlled at 38.5 ± 0.5 °C using a water circulating pad.

The visual stimulus was binocular, full-field, black and white square-wave, drifting gratings. The moving gratings had a spatial frequency of 0.15 cycle/degree and a temporal frequency of 2 cycles/s, and the orientation of the gratings varied from every 2 s in 45-degree steps. A gray screen was presented for the control.

MR experiments

All MRI experiments were performed on a 9.4-T/31-cm magnet (Magnex, UK), interfaced to a Unity INOVA console (Varian, Palo Alto, CA). The actively shielded 12-cm diameter gradient insert (Magnex, UK) operating at a maximum gradient strength of 40 gauss/cm and a rise time of 120 μs was used. From a multi-slice scout fMRI study, a coronal slice showing robust activation and good-quality echo-planar image (EPI) was chosen for subsequent fMRI studies, and a T_1-weighted FLASH image or spin-echo EPI image with a 128×128 matrix was obtained for anatomical reference. A surface coil with diameter of 1.6 cm was chosen to achieve high spatial resolution and high sensitivity, and also to reduce the power deposition during the long SL pulse.

Since surface coil excitation induces an inhomogeneous B_1 field, the B_1 map was measured using a square pulse (to replace the SL preparation pulse in Fig. 1), where the pulse length was incremented such that signal intensity oscillated for several cycles in each imaging voxel within the area of interest, and the frequency of this oscillation was obtained. The same B_1 was used for spin-locking ($B_{1, SL}$). Since the SL frequency ($v_{1, SL}$) is spatially inhomogeneous, SL frequencies in our text were referred to as the averaged value on the region of interest (ROI). For $T_{1\rho}$-weighted MRI studies, the non-selective excitation and refocus pulses (see Fig. 1) were calibrated to ensure that the adiabatic condition was achieved for most of the primary visual area. The validity of the $T_{1\rho}$ measurement with the adiabatic SL sequence using the surface coil was confirmed by phantom study with a conventional SL sequence using a homogeneous coil (data not shown).

All MRI experiments were acquired with a 2×2 cm^2 field of view and a 2-mm slice thickness. SL-prepared images were acquired using a two-segmented EPI with a matrix size of 96×96 and TR of 2.5 s per segment. The baseline CSF volume fraction (V_{csf}) was measured with TE = 15 ms and 15 TSL values of 0, 10, 20, 30, 40, 50, 60, 80, 100, 120, 150, 180, 225, 280, and 350 ms. For fMRI studies, runs with TSL/TE of 200/15 ms and 300/22.5 ms were interleaved; the runs with TSL/TE = 300/22.5 ms were repeated ~50% more than the runs with TSL/TE = 200/15 ms so that the SNR was similar for both sets of images. For 2 out of 6 animals, spin-echo BOLD fMRI with TR/TE = 2.5 s/22.5 ms (i.e. TSL = 0) were additionally acquired for comparison with $T_{1\rho}$-weighted fMRI. The visual stimulation paradigm consisted of 10 (50 s) control, 8 (40 s) stimulation, and 12 control images for each fMRI run and a 45-s resting time between runs.

Data analysis

Data were analyzed with in-house Matlab® programs and STIMULATE software (Strupp, 1996). For all MRI data, images were first zero-filled to 128×128 in k-space and then smoothed using a Gaussian filter with full-width at half maximum (FWHM) of 3 pixels to remove the Gibbs ringing artifacts. A baseline V_{csf} map was obtained by fitting the multi-TSL data to a two-exponential model on a pixel-by-pixel basis (Eq. (2)), using literature values: $\rho_{csf} = 1$, $\rho_{par} = 0.89$ (Lu et al., 2003), $T_{2,csf} = 180$ ms (Miraux et al., 2008), $T_{2, par} = 40$ ms (Lee et al., 1999), $T_{1,csf} = 4.3$ s, and $T_{1,par} = 2.0$ s (Kuo et al.,

2005). Despite the usage of a surface coil, spatial variation of $T_{1\rho}$ was very small in our study (as shown later); therefore, $T_{1\rho, par}$ of 48 ms and $T_{1\rho,csf}$ of 450 ms were used.

fMRI runs with same TSL/TE values were grouped together and averaged. Student's t-test was performed on a pixel-by-pixel basis to detect the activated area. First, a p-value threshold was chosen ($p < 0.05$, uncorrected for multiple comparisons), and a minimal cluster size of four pixels was applied. Then, a percentage signal change map was calculated on the activated pixels by comparing average signal intensities of 50-s pre-stimulus images versus images acquired during the stimulation period (i.e., 5–40 s after the stimulus onset). Data were also analyzed using the ROI, which was manually drawn at the surface of the visual cortex based on the anatomic image, regardless of whether these pixels passed the statistical threshold. For each activated pixel, the baseline V_{csf} value and the functional signal change were obtained and compared.

Results

Baseline V_{csf} determination

Since a surface coil was used for our experiments, an inhomogeneous B_1 field (Fig. 2B) was observed in the cat visual cortex. The $B_{1, SL}$ at an ROI close to the coil (560 Hz, blue square) is about 40% higher than that of another ROI farther from the coil (400 Hz, red square). However, the $R_{1\rho}$ ($= 1/T_{1\rho}$) map shows little spatial heterogeneity at the cortex (Fig. 2C), because the tissue $T_{1\rho}$ values do not vary significantly for the narrow $B_{1, SL}$ range of a few hundred Hz: the $T_{1\rho}$ value is 48.5 ms for the near-coil ROI, while it is 47.6 ms for the far-from-coil ROI. At low SL fields used for *in vivo* studies, $T_{1\rho}$ is much closer to the T_2 value than T_1 (T_1 and T_2 values of gray matter at 9.4 T are 2 s and 40 ms, respectively). The area between the two hemispheres contains CSF (dark pixels in Fig. 2C) with very small $R_{1\rho}$ values. The baseline $T_{1\rho,csf}$ was found to be 449 ± 37 ms ($n = 6$). Since $T_{1\rho}$ of CSF is much longer than that of the parenchyma (about 48 ms), the image contrast between CSF and parenchyma can easily be adjusted with TSL (e.g., TSL = 0 ms for Fig. 2D and 200 ms for Fig. 2E). With a 200-ms long TSL preparation pulse, the parenchyma signal dropped to ~1.6% of the signal with TSL = 0 ms (red square), whereas a significant portion (~60% of the signal with TSL = 0, purple arrows) of the CSF signal remained (Fig. 2E vs. 2D). The baseline V_{csf} map (Fig. 2F) was obtained from multiple TSL images with the two-compartment model (Eq. (2)), which appears similar to the highly $T_{1\rho}$-weighted image (Fig. 2E).

Functional ΔV_{csf} measurements

Without SL preparation (TSL = 0), the MR signal increases during activation at the brain parenchyma (Fig. 3A and F), as expected for the spin-echo BOLD contrast. In contrast, with a long TSL preparation, the signal change in the parenchyma cannot be detected, while the MR signal decreases at the boundary of the parenchyma/CSF interface (Fig. 3B, C, G and H). Generally, a decrease in relaxation rates due to the BOLD effect increases fMRI signals, while a reduction in CSF volume fraction decreases fMRI signals when the parenchyma signal is suppressed. These functional maps indicated that the former mechanism is dominant at the parenchyma for TSL = 0, while the latter is dominant at the parenchyma/CSF interface for long TSL data. The activation pattern and the number of activation pixels were similar for the two TSL values of 200 and 300 ms (Fig. 3B vs. C, and G vs. H). When these fMRI maps are compared with the baseline CSF volume fraction maps (Fig. 3D and I), the pixels with low baseline V_{csf} values tend to have high percentage signal changes (yellow arrows), whereas pixels with a high baseline V_{csf} have small or no fMRI signal changes (green arrows). Note that some pixels show an fMRI signal increase (red to yellow pixels), which is probably caused by a change in the inflow of spins from outside the coil coverage. The maps of absolute CSF volume fractional
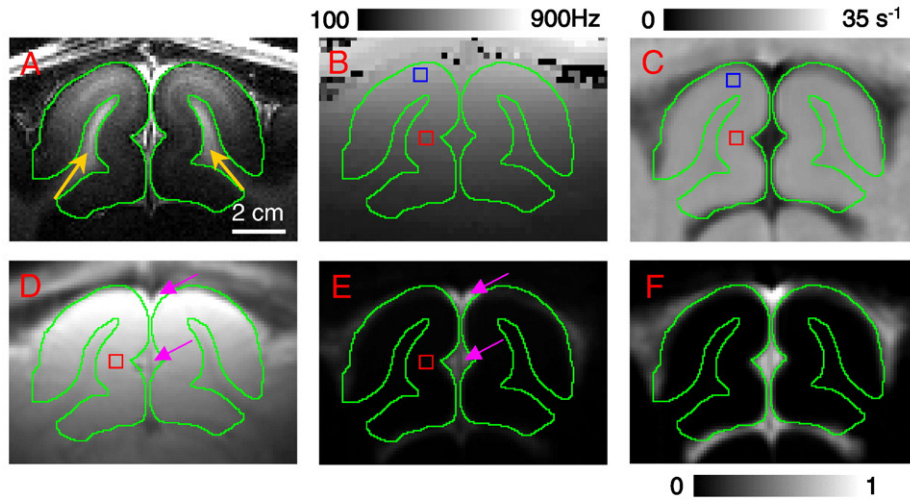
Fig. 2. Result of spin-lock MR images. In the T_1-weighted image of the cat visual cortex (A), the gray matter area is outlined in green and the white matter is indicated by the yellow arrows. With a surface coil, the v_1 map (B) shows large spatial inhomogeneity: the v_1 at a near-coil ROI (blue square) is 40% larger than that at a far-from-coil ROI (red square). $R_{1\rho}$ ($=1/T_{1\rho}$) was calculated by pixel-wise fitting of the image intensities to a mono-exponential decay as a function of the spin-locking time (TSL). The map of $R_{1\rho}$ (C) shows little spatial variation in the parenchyma. Compared to the EPI image without SL preparation (D), long SL preparation with TSL of 200 ms (E) suppressed the parenchymal signal. For visual comparison between D and E, the same intensity scale was used. Purple arrows: CSF. The baseline V_{csf} map obtained from a two-compartment model (F) appears similar to the raw EPI image with long SL preparation (E).

change were obtained by multiplying the baseline V_{csf} maps with the percentage signal change maps (for TSL = 300 ms). Compared with the percentage signal change maps (Fig. 3E vs. 3C and 3J vs. 3H), the magnitude of activation in the ΔV_{csf} maps appears more uniform.

A cortical surface ROI (Fig. 4A, inset) was chosen for time course analysis. On average ($n=6$), a $2.45 \pm 0.58\%$ signal decrease for TSL = 200 ms and TE = 15 ms and a $2.45 \pm 0.59\%$ for TSL = 300 ms and TE = 22.5 ms were observed from the ROI with an average size of 246 ± 41 pixels. The time courses also show that the signal changes are independent of TSL and TE values (Fig. 4), suggesting that the TSL- and TE-related terms in Eq. (4) are insignificant and that $\Delta V_{csf}/V_{csf}$ is dominant. The averaged baseline V_{csf} is $24.6 \pm 2\%$ ($n=6$) for the surface ROI, and the average absolute CSF volume fraction decreases by $0.6 \pm 0.15\%$ ($n=6$) during stimulation. For all activated pixels within the cortical surface ROI, a negative correlation exists between the percentage signal change and the baseline V_{csf}, as shown in Fig. 4B

for one representative dataset ($R=-0.55$ for TSL = 200 ms and -0.59 for TSL = 300 ms). On average ($n=6$), the correlation coefficient is $R=-0.54 \pm 0.08$ for TSL = 200 ms and -0.55 ± 0.07 for TSL = 300 ms. To explain our experimental data better, $\Delta S/S$ of $T_{1\rho}$-weighed fMRI was calculated as a function of baseline V_{csf} using Eq. (4) with a fixed ΔV_{csf} (-0.6%) and negligible relaxation terms. Simulated $\Delta S/S$ (the dashed line) is similar to experimental data, suggesting that ΔV_{csf} is similar across pixels in our selected ROI.

Discussion

Methodological considerations

We have shown that the *relative* functional change of CSF volume fraction can be imaged directly using a simple $T_{1\rho}$-weighted acquisition paradigm, without complex theoretical models and data
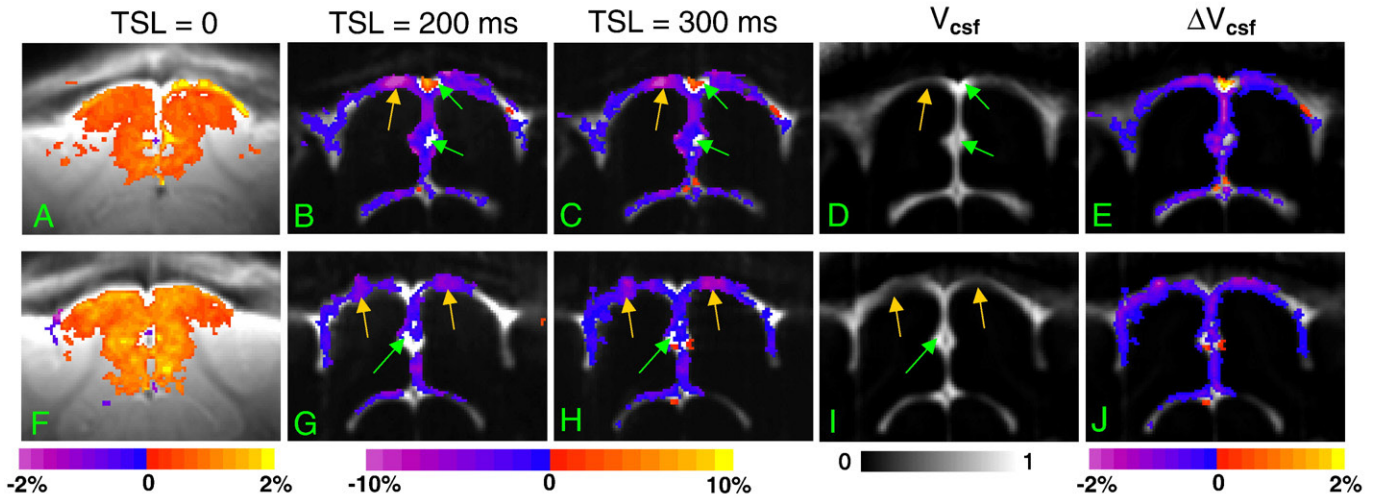

Fig. 3. $T_{1\rho}$-weighted fMRI studies of two representative animals (upper and lower panel). Percentage change maps of $T_{1\rho}$-weighted fMRI with TSL = 0 (A and F), 200 ms (B and G) and 300 ms (C and H) were overlaid on their respective baseline echo-planar images. Without $T_{1\rho}$ weighting, the spin-echo fMRI map shows an increase of BOLD signal at the parenchyma as expected (A and F). With long TSL, the fMRI signal decreases at the CSF area (blue to purple pixels) due to the reduction of CSF volume fractions. Pixels showing the highest and lowest negative percentage signal changes (yellow and green arrows, respectively) have low and high baseline V_{csf} values in the baseline V_{csf} maps, respectively (D and I). Consequently, the magnitudes of activation in absolute V_{csf} change maps (E and J) appear more uniform than the percentage signal change maps (compare between two color scales).
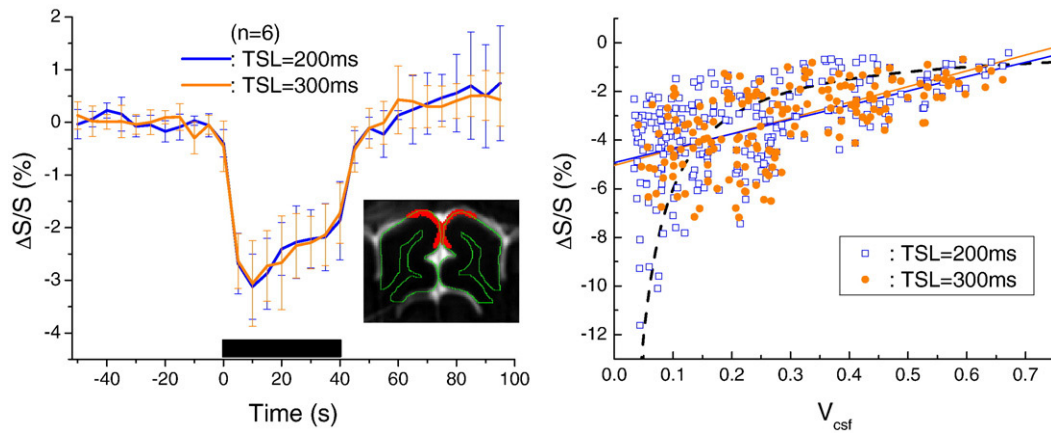
Fig. 4. (A) Averaged time courses of the fMRI runs with TSL/TE = 200/15 ms (blue line) and 300/22.5 ms (orange line) were obtained from the cortical surface ROI (red pixels) shown in inset image. These time courses are very similar, indicating minimal TSL- and TE-dependent signal contributions. Error bars show the standard deviations. (B) Baseline V_{csf} and $\Delta S/S$ were plotted for all pixels within the ROI in one representative animal. The percentage signal change is negatively correlated with the baseline CSF volume fraction (solid lines). Assuming absolute V_{csf} change of −0.6%, the $\Delta S/S$ value estimated from baseline V_{csf} is plotted as a dashed line.

fitting. This method utilizes the large difference between the tissue and CSF $T_{1\rho}$ (48 vs. 450 ms). As a comparison, the differences in the T_1 at 9.4 T (2 vs. 4.3 s) and the water diffusion coefficient (0.75 vs. 2.5×10^{-3} mm²/s) are much smaller. For an example, the CSF signal would be only $0.07 \cdot M_0$ if the parenchyma signal is nulled at 9.4 T with the inversion-recovery technique for TR = 2.5 s. Among conventional MR contrasts, T_2 offers a relatively large difference between the tissue and CSF (40 vs. 180 ms at 9.4 T) and is easier to implement than the SL technique. However, it is susceptible to the large field inhomogeneity around surface venous vessels; thus, it is necessary to acquire multiple TE data for measurement of functional CSF volume change. In a previous multi-TE spin-echo fMRI study with similar parameters as in this work but lower spatial resolution (Jin et al., 2006), a signal decrease of 0.27% was obtained at the cortical surface area when extrapolated to TE = 0, which can partially be attributed to the reduction of CSF volume fraction. In our single heavily $T_{1\rho}$-weighted fMRI, TE-dependent BOLD contribution was minimal. This can also be explained by our previous multi-TE spin-echo fMRI study (Jin et al., 2006), where an extravascular ΔR_2 of −0.2 s^{-1} was obtained at the cortical surface area, suggesting a 0.15% difference for the two scans with TE = 15 and 22.5 ms. This difference is much smaller than the observed change of −2.45% and can not be distinguished with the sensitivity in the current experiments.

In this study the *baseline* V_{csf} was obtained with two-compartment fitting. The similarity between Fig. 2E and F suggested that the baseline V_{csf} can also be obtained by a single TSL acquisition without multi-compartment fitting. With a highly $T_{1\rho}$-weighted image (e.g., with TSL ≥ 300 ms), the parenchymal term on the right-hand side of Eq. (2) is almost zero; the CSF volume fraction map may be obtained by normalization with the highest signal intensity (i.e., the voxel with the highest V_{csf}, which is assumed to be 1.0). However, we did not attempt to obtain a V_{csf} map with this method, because our small surface coil leads to two additional complications: (1) The B_1 field inhomogeneity is very large and should be corrected, and (2) the inflow effect may increase the signal intensity at certain pixels with large arteries, leading to potential error in normalization. These two issues may be avoided with volume coil acquisition.

Implication for fMRI

In our high-resolution cat studies, baseline V_{csf} for the surface ROI was 24.6%, and functional ΔV_{csf} was −0.6% during visual stimulation. The ΔV_{csf} maps are relatively uniform at the cortical surface/CSF boundary (Fig. 3E and J). Note that spin-echo BOLD maps (Fig. 3A and F) also appear fairly uniform across the cortex, however the

reason of this apparent similarity is unclear. In human visual stimulation studies, the baseline V_{csf} was reported to be ~10%, and the ΔV_{csf} decrease was on the order of 0.5–0.6% (Donahue et al., 2006; Piechnik et al., 2009). Although CSF volume fraction was observed to decrease during vascular activation, it is unclear whether this change of CSF volume fraction is solely caused by the dilation of vessels on the cortical surface, or there may also be significant contributions from the dilation of parenchymal vessels. The former mechanism will be valid if a local redistribution of tissue and blood water occurs within the brain parenchyma and the parenchymal volume remains constant, as proposed in the VASO method (Donahue et al., 2006). The latter mechanism will be valid if the volume change mainly occurs between blood (including parenchymal vessels) and the CSF compartment, while the tissue volume is relatively constant. In this case, the tissue water volume is shifted as a propagator to compress the CSF volume. Further studies are necessary to determine the exact source of CSF volume fraction reduction.

Shift between parenchyma (including tissue and blood) and CSF compartments may have important implications for fMRI signal depending on the relative weighting of the parenchyma and CSF signal in a voxel and, thus, also on experimental technique and parameters. To evaluate the impact of CSF volume fraction change to fMRI studies, we used a simple two-compartment model:

$$S = V_{csf} \cdot S_{csf} + (1 - V_{csf}) \cdot S_{par}, \tag{5}$$

where S_{csf} and S_{par} are the signal intensity of CSF and parenchymal compartment, respectively. Assuming no changes in S_{csf} and S_{par}, the simulated percentage signal change as a ratio of the parenchyma to CSF signal (S_{par}/S_{csf}) is shown in Fig. 5A for ΔV_{csf} from −0.2% to −1% with fixed baseline V_{csf} of 25% and in Fig. 5B for baseline V_{csf} from 5% to 40% with fixed ΔV_{csf} of −0.6%. The volume fraction change does not contribute to the signal change only when the signals of CSF and parenchyma are equal. Generally, the effect of volume fraction change is small in conventional fMRI experiments where the CSF signal is close to the parenchyma signal. In fact, such effect is negligible in our spin-echo BOLD acquisition (Fig. 3A and F) where the difference between CSF signal and parenchyma signal is only about 10%. However, the effect of volume fraction change will become significant when the CSF signal and parenchyma signal are highly disparate, especially in the case when the parenchyma signal is suppressed as compared to CSF. For example, when baseline V_{csf} is 10%, a CSF volume fraction decrease of 0.6% (red line in Fig. 5B) would contribute to about −0.6% to −3% to $\Delta S/S$ when the CSF signal is 2 to 10 times higher than the parenchymal signal. On the other hand, when the CSF signal is suppressed 2 to 10 times relative
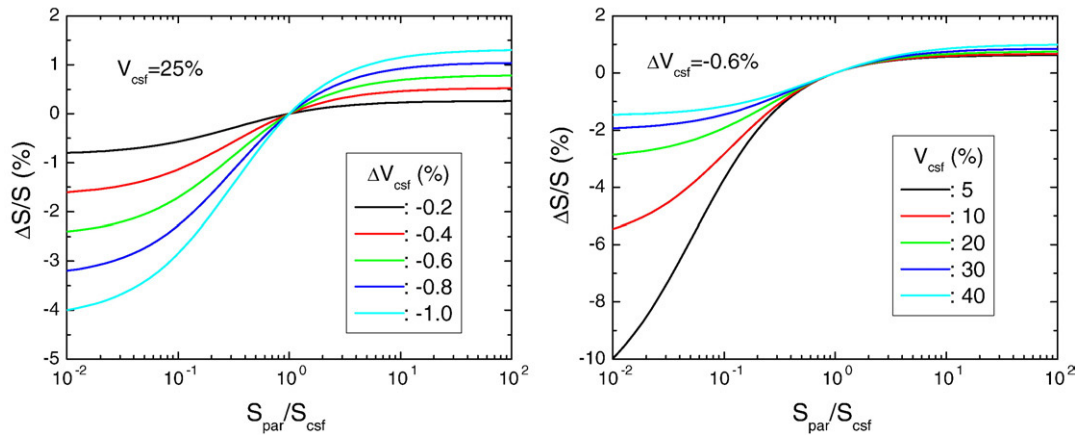
Fig. 5. fMRI signals solely induced by CSF and parenchyma volume fraction changes without the contribution of any hemodynamic changes. Eq. (5) was used for simulation of $\Delta S/S$ as a function of S_{par}/S_{csf}, where S_{par} and S_{csf} is the parenchyma and CSF signal intensity, respectively. A decrease in partial CSF volume fraction (V_{csf}) is accompanied with an increase in parenchyma volume fraction. Five ΔV_{csf} values ranging from -0.2% to -1% with fixed baseline V_{csf} of 25% (A) and baseline V_{csf} from 5% to 40% with fixed ΔV_{csf} of -0.6% (B) were used. Baseline V_{csf} of 24.6% and ΔV_{csf} of -0.6% were experimentally found in our cat visual stimulation studies.

to the parenchymal signal, this volume fraction change leads to a signal increase of 0.3% to 0.6%. Therefore, the CSF volume fraction change should be considered especially when the CSF signal intensity is much higher than the parenchymal signal because the fMRI signal change is on the order of a few percent (e.g., VASO or gray matter-nulled fMRI) (Donahue et al., 2006; Lu et al., 2003).

Conclusions

We have demonstrated that a long spin-locking preparation can be applied to image the CSF compartment directly and to robustly detect the functional decrease of CSF volume fraction during visual stimulation. The displacement of CSF and parenchyma would contribute greatly to the fMRI signal when the ratio of the CSF and parenchymal signals is deviated significantly from unity. In particular, care should be taken for quantitative fMRI techniques in which the parenchymal signal is significantly reduced as compared to the CSF.

Acknowledgments

References

Borthakur, A., Charagundla, S.R., Wheaton, A., Reddy, R., 2004. T-1ho-weighted MRI using a surface coil to transmit spin-lock pulses. J. Magn. Reson. 167, 306–316.

Donahue, M.J., Lu, H.Z., Jones, C.K., Edden, R.A.E., Pekar, J.J., van Zijl, P.C.M., 2006. Theoretical and experimental investigation of the VASO contrast mechanism. Magn. Reson. Med. 56, 1261–1273.

Grohn, H.I., Michaeli, S., Garwood, M., Kauppinen, R.A., Grohn, O.H.J., 2005. Quantitative T-1ρ and adiabatic Carr-Purcell T-2 magnetic resonance imaging of human occipital lobe at 4 T. Magn. Reson. Med. 54, 14–19.

Hakumaki, J.M., Grohn, O.H.J., Tyynela, K., Valonen, P., Yla-Herttuala, S., Kauppinen, R.A., 2002. Early gene therapy-induced apoptotic response in BT4C gliomas by magnetic resonance relaxation contrast T-1 in the rotating frame. Cancer Gene Ther. 9, 338–345.

Jin, T., Wang, P., Kim, S.G., 2009. Separation of the vascular and tissue contributions to the T1rho change induced by brain activation. Proc 17th Annual Meeting, ISMRM, Honolulu, Hawaii, p. P1577.

Jin, T., Wang, P., Tasker, M., Zhao, F.Q., Kim, S.G., 2006. Source of nonlinearity in echo-time-dependent BOLD fMRI. Magn. Reson. Med. 55, 1281–1290.

Koskinen, S.K., Niemi, P.T., Kajander, S.A., Komu, M.E.S., 2006. T-1rho Dispersion profile of rat tissues in vitro at very low locking fields. Magn. Reson. Imaging 24, 295–299.

Kuo, Y.T., Herlihy, A.H., So, P.W., Bhakoo, K.K., Bell, J.D., 2005. In vivo measurements of T1 relaxation times in mouse brain associated with different modes of systemic administration of manganese chloride. J. Magn. Reson. Imaging 21, 334–339.

Lee, S.-P., Silva, A.C., Ugurbil, K., Kim, S.-G., 1999. Diffusion-weighted spin-echo fMRI at 9.4 T: microvascular/tissue contribution to BOLD signal change. Magn. Reson. Med. 42, 919–928.

Lu, H., Golay, X., Pekar, J., Van Zijl, P., 2003. Functional magnetic resonance imaging based on changes in vascular space occupancy. Magn. Reson. Med. 50, 263–274.

Makela, H.I., De Vita, E., Grohn, O.H.J., Kettunen, M.I., Kavec, M., Lythgoe, M., Garwood, M., Ordidge, R., Kauppinen, R.A., 2004. B-0 dependence of the on-resonance longitudinal relaxation time in the rotating frame (T-1ρ) in protein phantoms and rat brain in vivo. Magn. Reson. Med. 51, 4–8.

Miraux, S., Massot, P., Ribot, E.J., Franconi, J.M., Thiaudiere, E., 2008. 3D TrueFISP imaging of mouse brain at 4.7 T and 9.4 T. J. Magn. Reson. Imaging 28, 497–503.

Piechnik, S.K., Evans, J., Bary, L.H., Wise, R.G., Jezzard, P., 2009. Functional changes in CSF volume estimated using measurement of water T-2 relaxation. Magn. Reson. Med. 61, 579–586.

Scouten, A., Constable, R.T., 2008. VASO-based calculations of CBV change: accounting for the dynamic CSF volume. Magn. Reson. Med. 58, 308–315.

Shen, Y., Kauppinen, R.A., Vidyasagar, R., Golay, X., 2009. A functional magnetic resonance imaging technique based on nulling extravascular gray matter signal. J. Cereb. Blood Flow Metab. 29, 144–156.

Strupp, J.P., 1996. Stimulate: A GUI based fMRI analysis software package. Neuroimage 3, S607.

Xu, S., Yang, J., Shen, J., 2008. In vivo T1rho-weighted MR imaging of rat brain using a surface coil at 11.7T. Proceedings of 16th ISMRM, Proceedings of 16th ISMRM, Toronto, Canada, p. 3077.